Brillouin interaction between single optical modes excited in multimode fibers

Andrei Fotiadi [a,b], Edik Rafailov [c], Dmitry Korobko [d], Ivan Chapalo [b], Patrice Mégret [b], Alexander Bykov [c], Igor Meglinski [c]

[a]Optoelectronics and Measurement Techniques Unit, University of Oulu, 90570 Oulu, Finland
[b]University of Mons, Boulevard Dolez 31, 7000 Mons, Belgium.
[c]Optoelectronics and Biomedical Photonics Group, School of Engineering and Applied Science, Aston University, Birmingham, B4 7ET, U.K.
[d]Ulyanovsk State University, 42 Leo Tolstoy Street, Ulyanovsk, 432970, Russia.

ABSTRACT

A multimode optical fiber supports excitation and propagation of a pure single optical mode, i.e., the field pattern that satisfies the boundary conditions and does not change along the fiber. When two counterpropagating pure optical modes are excited, they could interact through the stimulated Brillouin scattering (SBS) process. Here, we present a simple theoretical formalism describing SBS interaction between two individual optical modes selectively excited in an acoustically isotropic multimode optical fiber. Employing a weakly guiding step-index fiber approach, we have built an analytical expression for the spatial distribution of the sound field amplitude in the fiber core and explored the features of SBS gain spectra, describing the interaction between modes of different orders. In this way, we give a clear insight into the sound propagation effects accompanying SBS in multimode optical fibers, and demonstrate their specific contributions to the SBS gain spectrum.

Keywords: Multimode optical fiber; stimulated Brillouin scattering; optical fiber amplifiers; mode-division multiplexing; Brillouin imaging; distributed Brillouin sensing

INTRODUCTION

Stimulated Brillouin scattering (SBS) is embedded today in various optical systems, such as advanced low-noise lasers, distributed fiber sensors, microwave signal processors, scientific instrumentation, and optomechanical systems [1]. Some of these applications are tied to particular attributes of SBS in single-mode optical fibers: narrow-band optical amplification, linewidth narrowing, random and narrow-band lasing, controllable light coherency, optical signal processing, etc. The use of multimode fibers as SBS media extends these functionalities, engaging the effects of nonlinear optical mode conversion and optical phase conjugation [2, 3] and leading to a new generation of high-performance fiber devices. Brillouin-distributed sensing based on multimode fibers enables the optical Vernier effect [4] that relies on the use of several similar sensors with slightly detuned properties, providing a significant magnification of the sensing capabilities, e.g., by magnifying the measured Brillouin frequency shift compared to a classical BOTDA system [5]. Recently, Brillouin imaging (BI) has become a valuable tool for micromechanical material characterization, thanks to extensive progress in optical fiber instrumentation [6, 7]. This powerful technique is contactless and label-free, making it especially suitable for biomedical applications [8]. Randomized light fields [9, 10] also open up new forms of optical imaging based on Brillouin scattering. A standard multimode optical fiber provides randomized light propagation, whereas random lasing [11-13] is available through the Rayleigh–Brillouin cooperative process [14].

Multimode optical fibers enable significant progress in modern sensing and imaging techniques that point to miniaturization technologies. A standard multimode optical fiber can be used as a general-purpose spectrometer after calibrating the wavelength-dependent speckle patterns produced by interference between the guided modes of the fiber [15, 16]. Multimode fiber endoscopes with minimal invasiveness are developed for in vivo applications such as 3D imaging, mechanical mapping, ablation of cancerous cells, intraoperative monitoring and optogenetic cell stimulation. They do not require any optical or electro-mechanical elements on the distal fiber end, and can deliver three-dimensional information without pixelation by exploiting wavefront shaping. High-frequency real-time ultrasound imaging [17] can provide exquisite visualizations of tissue to guide minimally invasive procedures. With this device, broad-bandwidth ultrasound generation is achieved through the photoacoustic excitation of a special composite coating on the distal end of the multimode optical fiber by a pulsed laser [18]. Although most commercial sensing systems rely on measurements of the

transmitted or reflected fundamental mode of single-mode optical fibers [19-23], more recent developments have focused on multimodal architectures that considerably widen the sensing modalities, especially in the chemical and biological fields [24-28]. Mode–division multiplexing is mooted to address the possibility of multiparameter sensing with a single device, the reduction of cross-sensitivities, and the improved accuracy of a single measured parameter by combining the responses of many fiber modes to its evolution. Current progress in mode–division multiplexing relies on the elaboration of new tools for encoding and de-encoding the information stored in the spatial modes of fibers [29, 30]. Stimulated Brillouin scattering (SBS) is able to assist all these new paradigms, enabling selective mode amplification, mode conversion and inter-mode signal processing to be implemented immediately inside the multimode optical fibers.
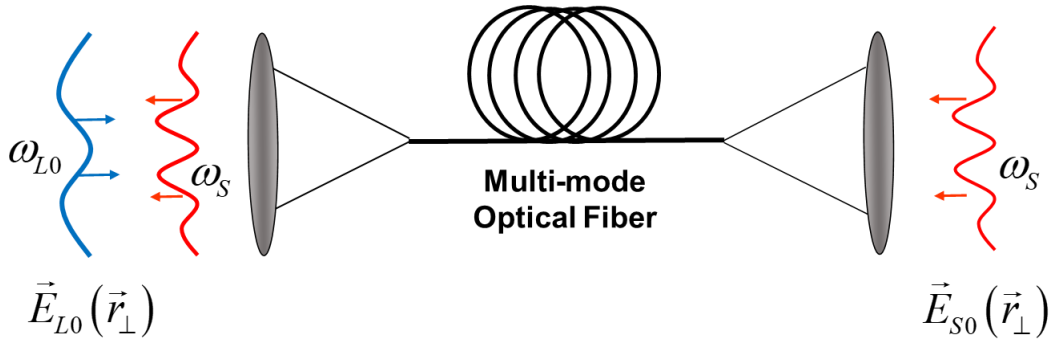

Figure 1. Brillouin amplification process in multimode optical fiber. The optical fields with specific profiles $\vec{E}_{L0}(\vec{r}_\perp)$ and $\vec{E}_{S0}(\vec{r}_\perp)$ at frequencies ω_L and ω_S are introduced into the multimode optical fiber, providing selective excitation of pure pump $\vec{e}_L(\vec{r}_\perp)\exp\{i[\omega_L t - \beta_L z]\}$ and Stokes $\vec{e}_S(\vec{r}_\perp)\exp\{i[\omega_S t + \beta_S z]\}$ optical modes. Their interaction inside the optical fiber with the sound wave leads to amplification of the Stokes mode amplitude.

Stimulated Brillouin scattering in multimode fibers has been previously studied in the context of the optical phase conjugation effect [2,3,23,24], laser beam combining and cleanup [31]. In particular, the earliest experiments have demonstrated significant difference in the SBS gain factors measured with the optical modes of different orders excited in the same optical fiber sample [32]. The efficiency of the stimulated Brillouin scattering (SBS) process in multimode optical fibers is largely governed by the spatial overlap between the supported optical and acoustic modes leading to a complicated amalgamation of photon–phonon interactions in multimode fibers [33]. Here, we present theoretical formalism to describe SBS dynamics in multimode optical fibers using the weakly guiding step-index optical fiber approach [34]. In contrast to previous studies [35-41], we consider a simplified situation in which the optical fiber is acoustically uniform and only two counter-propagating pure optical modes are excited and interact inside the fiber, as shown in Fig. 1. Interaction between these modes is characterized by an SBS gain spectrum inherent to the interacting mode pair. We have managed to build an analytical expression for the spatial distribution of the sound wave amplitude over the fiber core, and highlight the features of the SBS gain spectrum specifically for interaction between modes of different orders. In this way, we give a clear insight into the sound propagation effects accompanying SBS in multimode optical fibers and demonstrate their specific contributions to the SBS gain spectrum, particularly to the spectrum broadening and splitting in the case of high-order mode interaction. For better understanding of the explored mechanisms, the effects obtained for SBS in optical fiber are compared with similar effects obtained for SBS in a volume medium and planar waveguide [42].

2. 3-D STEADY-STATE SBS MODEL

Let us consider an arbitrary optical fiber (or waveguide) with the input monochromatic pump and Stokes fields shown in Fig. 1. We assume that these complex fields are shaped by spatial light modulators and injected into the multimode fiber to excite a pair of pure single eigenmodes. The pump frequency ω_L is fixed, whereas the frequency of the Stokes wave ω_S is tunable. The input pump signal at ω_L excites the eigenmode $\vec{e}_L(\vec{r}_\perp)\exp\{i[\omega_L t - \beta_L z]\}$ with propagation constant β_L, and the input Stokes signal at ω_S excites the eigenmode $\vec{e}_S(\vec{r}_\perp)\exp\{i[\omega_S t + \beta_S z]\}$ with propagation constant β_S in a backward direction. It is convenient to characterize the Stokes wave frequency using its dimensionless detuning frequency $\delta = (\omega_S - \omega_{S0})T_2$, where $\omega_{S0} = \omega_L - \Omega_0$, $\Omega_0 = 2\upsilon n/c$, n is the waveguide core

refractive index, c is the velocity of light, υ is the sound wave velocity, and T_2 is the sound relaxation time[43]. So, the value $\delta = 0$ is the resonant SBS frequency shift corresponding to the interaction between two strictly counterpropagating optical plane waves in the volume medium with the same parameters.

To describe steady-state Brillouin amplification of the Stokes mode in the field of the given pump mode, we express the pump, Stokes, and sound wave fields as:

$$\vec{E}_L(\vec{r}_\perp, z) = A_L \cdot \vec{e}_L(\vec{r}_\perp) \exp\{i[\omega_L t - \beta_L z]\}$$

$$\vec{E}_S(\delta, \vec{r}_\perp, z) = A_S(\delta, z) \cdot \vec{e}_S(\vec{r}_\perp) \exp\left\{i\left[\left(\omega_{S0} + \frac{\delta}{T_2}\right)t + \beta_S z\right]\right\} \qquad (1)$$

$$P(\delta, \vec{r}_\perp, z) = A_L \cdot A_S^*(\delta, z) \cdot p(\delta, \vec{r}_\perp) \exp\left\{i\left[\left(\Omega_0 - \frac{\delta}{T_2}\right)t - (\beta_L + \beta_S)z\right]\right\}$$

Here, A_L, $A_S(\delta, z)$ and $A \cdot B^*(\delta, z) \cdot p(\delta, \vec{r}_\perp)$ are the complex amplitudes of the interacting fields; $p(\delta, \vec{r}_\perp)$ describes the distribution of the sound wave amplitude in the fiber cross-section, $\vec{r}_\perp = (x, y) = (r, \varphi)$ is the transvers fiber cross-section vector (to be described in Cartesian or cylindrical coordinates), and z is the coordinate along the fiber.

Near the resonance, the complex amplitude of the backward Stokes wave is amplified along z as:

$$A_S(\delta, z) = A_S(\delta, L) \exp\left\{G(\delta) \frac{g_0}{2} \frac{P_L}{S}(L - z)\right\}, \qquad (2)$$

where $P_L = A_L A_L^*$ is the pump power, L is the fiber length, S is the fiber core cross-section area $S = \iint_{core} dS = \iint_{core} r\, dr\, d\varphi = \iint_{core} dx\, dy$, and g_0 is the SBS power gain factor.

The normalized gain factor $G(\delta)$ in Eq. 2 reads as:

$$G(\delta) = \frac{1}{\hat{N}_L \hat{N}_S} \iint_{core} p(\delta, \vec{r}_\perp)\left(\vec{e}_L(\vec{r}_\perp) \cdot \vec{e}_S^*(\vec{r}_\perp)\right) dS, \qquad (3)$$

where $\hat{N}_i = \iint_{core}\left(\vec{e}_i(\vec{r}_\perp) \cdot \vec{e}_i^*(\vec{r}_\perp)\right) dS$ are mode power normalization constants. It is worth noting that $\mathrm{Re}\left[G(\delta)\right]$ describes the SBS gain spectrum.

Using Eqs. 1-3, the steady-state SBS problem[44] is reduced to the equation describing the cross-section profile of the acoustic wave amplitude $p(\delta, \vec{r}_\perp)$:

$$\left(1 + i(\delta - \delta_{LS})\right) p(\delta, \vec{r}_\perp) - i\mu \nabla_\perp p(\delta, \vec{r}_\perp) = \left(\vec{e}_L^*(\vec{r}_\perp) \cdot \vec{e}_S(\vec{r}_\perp)\right) \qquad (4)$$

where $\mu = \upsilon^2 T_2 / 2\Omega_0$ and $\delta_{LS} = T_2\left(\Omega_0 - \upsilon(\beta_L + \beta_S)\right)$.

In the next section, we consider the analytical solution of Eq. 4 describing the SBS interaction between two eigenmodes excited in a weakly guided step-index optical fiber. All calculations hereinafter are performed assuming that the optical fiber is pure silica; the optical fiber has a waveguide parameter $V \sim 55$, the parameter is $\mu \sim 0.0009$, the fiber core diameter is ~ 50 μm and the laser operation wavelength is ~ 1064 nm. It is worth noting that the last two parameters are used just to estimate the interaction angles α_L and α_S.

3. ANALITICAL SOLUTIONS FOR A CYLINDRICAL OPTICAL FIBER

To describe SBS interaction between individual optical modes in an optical fiber, based on Eqs. 1–4, the explicit expressions for fiber modes $\vec{e}_L(r, \varphi)$, $\vec{e}_S(r, \varphi)$ should be specified. We use the approximation of weakly guiding step-index cylindrical fibers ($\Delta = 1 - n_{core}/n_{clad} << 1$, where n_{core}, n_{clad} are the refractive index of the core and cladding) [34]. There are $\sim V^2/2$ guided modes that are characterized by their own orbital l and radial p parameters for the optical fiber with a numerical aperture NA, a core radius a and parameter $V = 2\pi \frac{a}{\lambda} NA$. At $l = 0$, for each $i = \{0, p\}$, there are two modes:

1. Even modes $HE_{1,p}$: $\vec{e}_{1,0,p}(\vec{r}) = \vec{x}\,\mathrm{J}_1\left(u_l^{1,p}r\right)$

2. Odd modes $HE_{1,p}$: $\vec{e}_{3,0,p}(\vec{r}) = \vec{y}\,\mathrm{J}_1\left(u_l^{3,p}r\right)$

At $l \geq 1$, for each $i = \{l,p\}$, there are four modes:

1. Even modes $HE_{l+1,p}$: $\quad \vec{e}_{1,l,p}(\vec{r}_\perp) = \{\vec{x}\cos(l\varphi) - \vec{y}\sin(l\varphi)\}\mathrm{J}_l\left(u_l^{1,p}r\right)$

2. Even modes $EH_{l-1,p}$: $\vec{e}_{2,l,p}(\vec{r}_\perp) = \{\vec{x}\cos(l\varphi) + \vec{y}\sin(l\varphi)\}\mathrm{J}_l\left(u_l^{2,p}r\right)$

3. Odd modes $HE_{l+1,p}$: $\vec{e}_{3,l,p}(\vec{r}_\perp) = \{\vec{x}\sin(l\varphi) + \vec{y}\cos(l\varphi)\}\mathrm{J}_l\left(u_l^{3,p}r\right)$

4. Odd modes $EH_{l-1,p}$: $\vec{e}_{4,l,p}(\vec{r}_\perp) = \{\vec{x}\sin(l\varphi) - \vec{y}\cos(l\varphi)\}\mathrm{J}_l\left(u_l^{4,p}r\right)$

Here, $\mathrm{J}_l\left(u_l^{s,p}r\right)$ denotes Bessel functions to be a solution of the characteristic equations $u\,\mathrm{J}_{l+1}(u)/\mathrm{J}_l(u) = \pm w\,\mathrm{K}_{l+1}(w)/\mathrm{K}_l(w)$, where $w = \sqrt{V^2 - u^2}$ gives sets of radial phase parameters $u_l^{1,p} \equiv u_l^{3,p}$ (sign +) and $u_l^{2,p} \equiv u_l^{4,p}$ (sign -), where p is the ordinal number of the solution in ascending order.

All even modes have different propagation constants, $\beta_l^{1,p}$ and $\beta_l^{2,p}$. All odd modes have the same propagation constants as the corresponding even modes. At $l = 1$, the propagation constants for all modes are different. The propagation constants $\beta_l^{1,p}$ and $\beta_l^{2,p}$ differ by $\sim \Delta^{3/2}\beta_l^p$. We can specify the modes as $m = \{l,p,s\}$, where $s = 1...4$ is the type of the mode in the given classification.

Now we have to substitute the expressions for pump and Stokes optical modes into Eq. 4 to consider its analytical solution. The pump and Stokes modes are determined by the sets of indexes $L = \{l_L, p_L, s_L\}$ and $S = \{l_S, p_S, s_S\}$, respectively, where l_L, l_S and p_L, p_S are orbital and radial optical mode parameters, and s_L, s_S set the type of the mode. Considering the interaction between two arbitrary pump and Stokes modes, we denote $u_L = u_{l_L}^{s_L,p_L}$, $u_S = u_{l_S}^{s_S,p_S}$ and express the scalar product $\left(\vec{e}_L^* \cdot \vec{e}_S\right) = \mathrm{J}_{l_L}(u_L r)\mathrm{J}_{l_S}(u_S r)f(\varphi)$, where $f(\varphi)$ is the function defined in Table 1 for modes of odd and even types. The sign (+ or -) between l_L and l_S in the expression for $f(\varphi)$ is important, so we distinguish $f^-(\varphi)$ and $f^+(\varphi)$.

Table 1. The function $f(\varphi)$ for different types of pump/Stokes modes used for SBS interaction.

Pump\Stokes	1. Even mode $HE_{l+1,p}$	2. Even mode $EH_{l-1,p}$	3. Odd mode $HE_{l+1,p}$	4. Odd mode $EH_{l-1,p}$
1. Even mode $HE_{l+1,p}$	$\cos(l_L - l_S)\varphi$	$\cos(l_L + l_S)\varphi$	$-\sin(l_L - l_S)\varphi$	$\sin(l_L + l_S)\varphi$
2. Even mode $EH_{l-1,p}$	$\cos(l_L + l_S)\varphi$	$\cos(l_L - l_S)\varphi$	$\sin(l_L + l_S)\varphi$	$-\sin(l_L - l_S)\varphi$
3. Odd mode $HE_{l+1,p}$	$\sin(l_L - l_S)\varphi$	$\sin(l_L + l_S)\varphi$	$\cos(l_L - l_S)\varphi$	$-\cos(l_L + l_S)\varphi$
4. Odd mode $EH_{l-1,p}$	$\sin(l_L + l_S)\varphi$	$\sin(l_L - l_S)\varphi$	$-\cos(l_L + l_S)\varphi$	$\cos(l_L - l_S)\varphi$

Then, using $p(r,\varphi) = \rho(r)f(\varphi)$, we separate the variables in Eq. 4, thus obtaining the equation describing the radial distribution of sound wave amplitude $\rho(r)$:

$$\left(1 + i(\delta - \delta_{LS})\right)\rho(\delta,r) -$$

$$-i\mu\left[\frac{d^2}{dr^2} + \frac{1}{r}\frac{d}{dr} - \frac{(l_L \pm l_S)^2}{r^2}\right]\rho(\delta,r) = \mathrm{J}_{l_L}(u_L r)\mathrm{J}_{l_S}(u_S r) \qquad (5)$$

where the sign in $l_L \pm l_S$ is taken as in $f^\pm(\varphi)$.

The ref. [42] expresses the solution of Eq. 5 in the form of an infinite series:

$$\left[\begin{array}{ll} \rho(\delta,r) = \sum_{m=-\infty}^{+\infty} C_m(\delta)\,\mathrm{J}_{l_L+m}(u_L r)\,\mathrm{J}_{l_S+m}(u_S r) & \text{for } f^{(-)}(\varphi) \\[2mm] \rho(\delta,r) = \sum_{m=-\infty}^{+\infty} (-1)^m C_m(\delta)\,\mathrm{J}_{l_L-m}(u_L r)\,\mathrm{J}_{l_S+m}(u_S r) & \text{for } f^{(+)}(\varphi) \end{array}\right. \tag{6}$$

In Eq. 6 the coefficients $C_m(\delta)$ are the functions of the frequency δ expressed as

$$C_m(\delta) = a^m \frac{\sqrt{x}\{[\cos m\phi + xd\sin m\phi] + i[\sin m\phi - xd\cos m\phi]\}}{x^2 d^2 + 1} \tag{7}$$

with the parameters as the following:

$$d(\delta) = \delta - \mu(u^2 + v^2)$$

$$c = uv\mu$$

$$a = \sqrt{\frac{1 - \sqrt{x}}{1 + \sqrt{x}}}$$

$$\phi = \arccos\left(\frac{d}{c}\frac{a}{a^2+1}\right)\mathrm{sign}\left(\frac{1}{c}\frac{a}{1-a^2}\right) \tag{8}$$

$$x = \frac{d^2 + 1 + \sqrt{D} - 4c^2}{d^2 + 1 + \sqrt{D} + 4c^2}$$

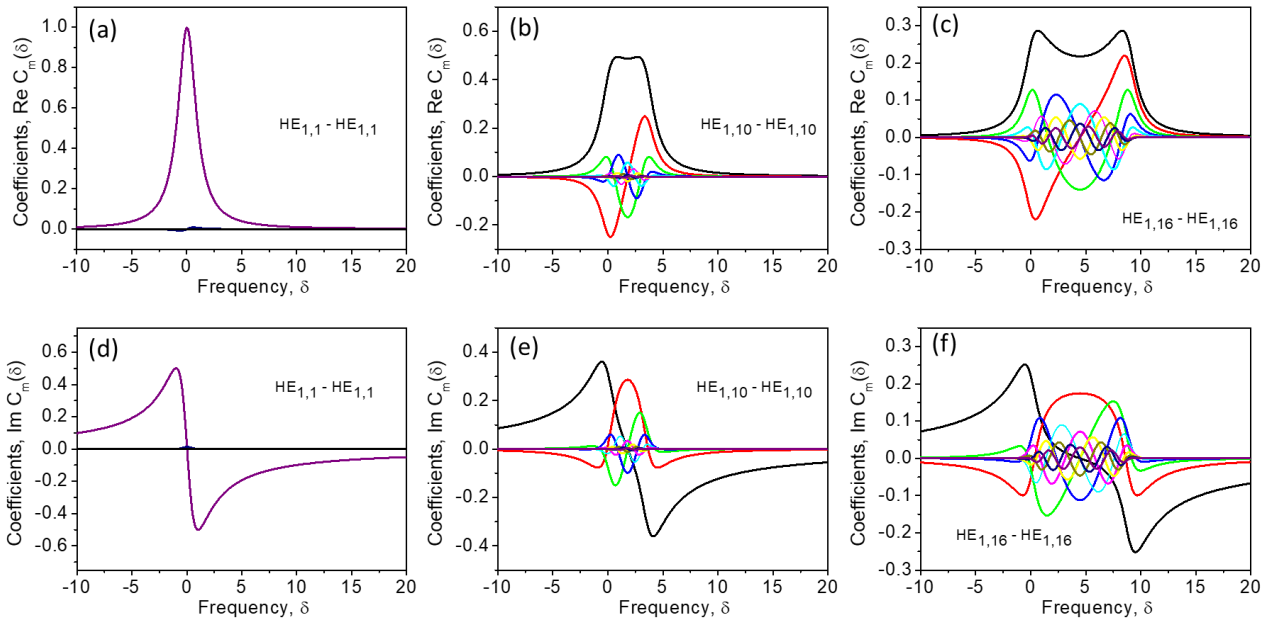$$D = d^4 + 16c^4 - 8c^2 d^2 + 2d^2 + 8c^2 + 1$$

Figure 2. The coefficients $C_m(\delta)$ ($m = 1, 2...10$) as functions of the frequency δ for interaction of the modes of different orders (a-c, d-f) in an optical fiber; the real (a-c) and imaginary (d-f) parts.

Substituting Eq. 7 into Eq. 6 for $\rho(r)$ and using an appropriate function $f(\varphi)$ from Table 1, one can obtain an analytical expression describing the distribution of the sound wave amplitude over the fiber cross-section $p(r,\varphi) = \rho(r)f(\varphi)$ for the case of a Brillouin interaction between an arbitrary pair of pump and Stokes optical fiber

modes. The azimuthal distribution of sound amplitude is trivial, and is determined by the orbital indices of the interacting modes only. The radial distribution $\rho(\delta, r)$ is represented as an infinite sum of Bessel function products with weight coefficients $C_m(\delta)$ (Eq. 7). Since $C_m(\delta) \sim a^m$ and $|a| < 1$, the sum converges. Commonly 10–20 terms are enough to calculate $\rho(\delta, r)$ in Eq. 6. Fig. 2 demonstrates several first coefficients $C_m(\delta)$ in the case of an interaction between the pump and Stokes modes of low (a, d), moderate (b, e) and high (c, f) orders. One can see that in the last case, the series $C_m(\delta)$ converges more slowly.
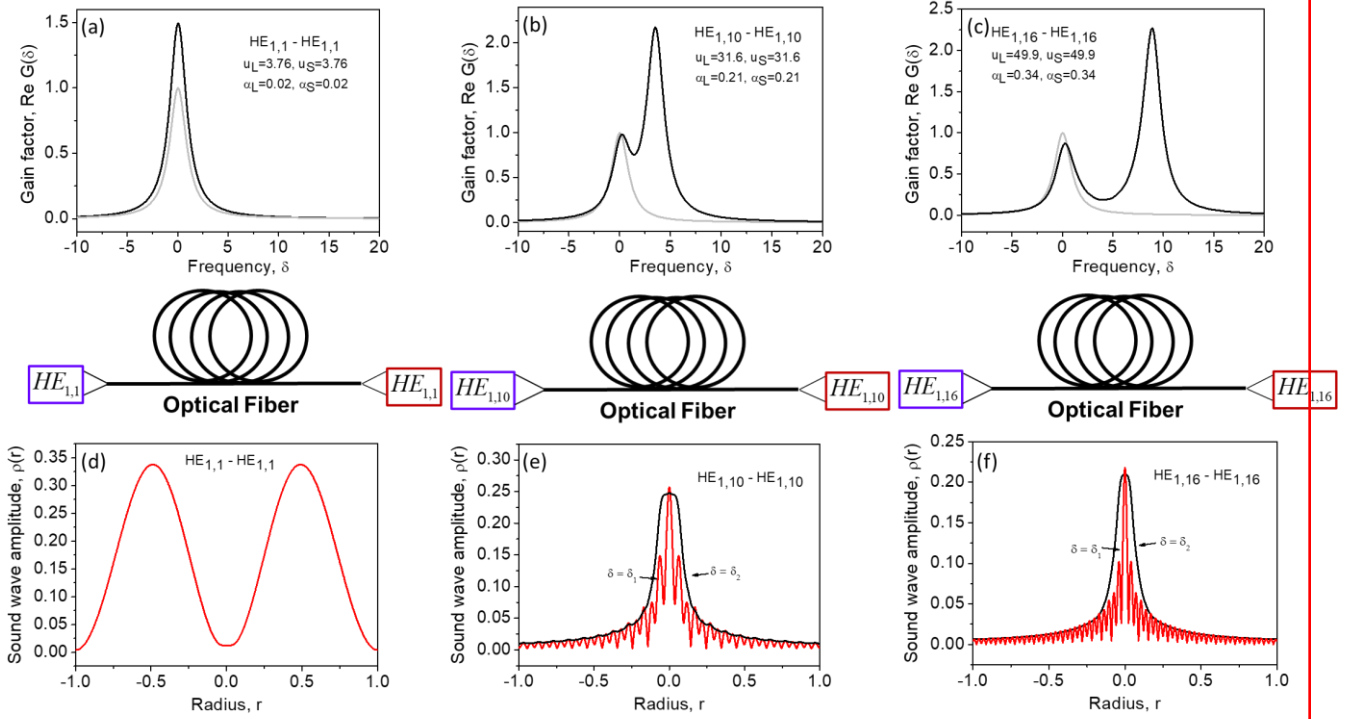

Figure 3. The SBS gain spectra $G(\delta)$ (a-c) and radial distribution of the sound amplitude $\rho(\delta, r)$ (d-f) at the frequencies δ corresponding to the left (red curve) and right (black curve) peak of the SBS gain spectra for interaction of modes of different orders (a-c, d-f) in an optical fiber.

Then substituting the expression for $\rho(\delta, r)$ and $f(\varphi)$ into Eq. 3, we come to the solution for the SBS gain spectrum in the form:

$$G(\delta) = K_\phi(s_L, s_S, l_L, l_S) \sum_{m=-\infty}^{\infty} C_m(\delta) K^{\pm r}(l_L, l_S, p_L, p_S, m) \qquad (9)$$

where the sign (+) or (-) is chosen as in $f^\pm(\varphi)$, $N_L = \int_0^1 \left[J_{l_L}(u_L r) \right]^2 r dr$ and $N_S = \int_0^1 \left[J_{l_S}(u_L r) \right]^2 r dr$ are normalization coefficients, and other parameters are

$$K^{-r}(l_L, l_S, p_L, p_S, m) = \frac{1}{N_L N_S} \int_0^1 \left[J_{l_L}(u_L r) J_{l_S}(u_S r) J_{l_L+m}(u_L r) J_{l_S+m}(u_S r) \right] r dr$$

$$K^{+r}(l_L, l_S, p_L, p_S, m) = \frac{(-1)^m}{N_L N_S} \int_0^1 \left[J_{l_L}(u_L r) J_{l_S}(u_S r) J_{l_L-m}(u_L r) J_{l_S+m}(u_S r) \right] r dr \qquad (10)$$

$$K_\phi(s_L, s_S, l_L, l_S) = \frac{1}{4\pi} \int_0^{2\pi} f_{l_L, l_S}^2(\phi) d\phi$$

Note that all coefficients expressed by Eqs. 10 are real. They are completely defined by the fiber parameters, and for the given fiber should be tabulated just once. The values of $K_\phi(s_L, s_S, l_L, l_S)$ for interacting modes of different types and orbital moments are presented in Table 2.

Table 2. The coefficient $4K_\phi(s_L, s_S, l_L, l_S)$ for different types of interacting modes.

Pump\Stokes	1. Even mode $HE_{l+1,p}$	2. Even mode $EH_{l-1,p}$	3. Odd mode $HE_{l+1,p}$	4. Odd mode $EH_{l-1,p}$
1. Even mode $HE_{l+1,p}$	$1 + \delta_{l_L, l_S}$	1	$1 - \delta_{l_L, l_S}$	1
2. Even mode $EH_{l-1,p}$	1	$1 + \delta_{l_L, l_S}$	1	$1 - \delta_{l_L, l_S}$
3. Odd mode $HE_{l+1,p}$	$1 - \delta_{l_L, l_S}$	1	$1 + \delta_{l_L, l_S}$	1
4. Odd mode $EH_{l-1,p}$	1	$1 - \delta_{l_L, l_S}$	1	$1 + \delta_{l_L, l_S}$

Importantly, the coefficients $C_m(\delta)$ accumulate all dependence on the frequency δ. Their linear combinations form both the gain spectrum profile $G(\delta)$ and the radial distribution $\rho(\delta, r)$ as a function of δ. The sum in Eq. 9 for the gain profile $G(\delta)$ converges as fast as the sum in Eq. 6, describing the sound amplitude.

4. BRILLOUIN INTERACTION BETWEEN THE MODES OF DIFFERENT ORDERS

One can see from Fig. 2 that the number of terms required for precise characterization of the Brillouin process through Eqs. 6 and 9 depends on the parameter μ that evaluates the strength of the sound propagation effects accompanying the Brillouin amplification process in optical fiber. Indeed, at $\mu(u_L^2 + u_S^2) \to 0$, all coefficients $C_m(\delta) \to 0$, except $C_0(\delta)$, and the spatial distribution of the sound amplitude $p(\delta, \vec{r}_\perp) = \dfrac{\vec{e}_L^*(\vec{r}_\perp) \cdot \vec{e}_S(\vec{r}_\perp)}{(1 + i\delta)}$, with some weight determined by δ, coincides with the parent interference pattern $\vec{e}_L^*(\vec{r}_\perp) \cdot \vec{e}_S(\vec{r}_\perp)$. As $\mu(u_L^2 + u_S^2)$ increases, more and more neighboring components $\sim J_{l1\pm m}(u_L r) J_{l2+m}(u_S r)$ become significant in the expansion (Eq. 6), causing a mismatch between the spatial distribution of sound amplitude $\rho(\delta, r)$ and the parent interference pattern $\vec{e}_L^*(\vec{r}_\perp) \cdot \vec{e}_S(\vec{r}_\perp)$. This mismatch reduces the efficiency of Brillouin interaction in optical fiber. This is in contrast with the SBS in a planar waveguide that produces the sound amplitude which is always coinciding with the parent interference pattern. [42]

Figure 3 shows the SBS gain spectra calculated for different interacting mode pairs (a-c) using Eq. 9 and radial distributions of the sound amplitude $\rho(\delta, r)$ (d-f) at peak δ values, using Eq. 6. At $\mu(u_L^2 + u_S^2) \ll 1$, in the case of interaction between two low-order modes, the gain spectrum shown in Fig. 3 (a) has only one peak at $\delta = 0$, with a width of $\Delta \nu_S \sim \dfrac{1}{\pi T_2}$ ($\Delta \delta \sim 1$). A single peak SBS gain spectrum shown in Fig. 3 (a) is similar to that for the SBS in a planar waveguide at small incident angles [42], but the maximal SBS gain exceeds the SBS factor for a volume medium more than twice. This is due to nonuniform (bell-like) distribution of the pump power in the fiber core which reduces the effective fiber core area available for nonlinear interaction. The radial distribution of the peak sound amplitude at $\delta = 0$ is shown in Fig. 3 (d). One can see that it exhibits a low spatial nonuniformity, but it is not a purely uniform distribution as in the case of the planar waveguide (for small incident angles, when the sound plane wave wavevector is parallel to z).

In the case of interaction between two high-order modes (b, c) the SBS gain spectrum exhibits two peaks. The peak observed at higher frequency $\delta_2 = \mu(u_L + u_S)^2$ is associated with pump scattering from the sound wave component $\rho(\delta_2, r)$, possessing lower transverse inhomogeneity (e, f, black curves). The peak of the SBS gain spectrum at the

lower frequency $\delta_1 = \mu\left(u_L - u_S\right)^2$ is associated with scattering from the sound wave component $\rho\left(\delta_1, r\right)$, possessing higher transverse inhomogeneity (e, f, red curves). These features are similar to that reported for the sound waves with high $\vec{q}_{1\perp}$ and low $\vec{q}_{2\perp}$ spatial frequencies in the case of a planar waveguide [42]. However, in contrast to the case of planar waveguide, two peaks of the SBS gain spectrum in an optical fiber possesses different amplitudes. The SBS gain peak at $\delta_2 = \mu\left(u_L + u_S\right)^2$ is always higher than that at $\delta_1 = \mu\left(u_L - u_S\right)^2$. This specific feature is attributed to the sound propagation effect illustrated in Fig. 2. At lower frequency $\delta = \delta_1$, the SBS interaction is governed by the sound wave component with higher transverse inhomogeneity that acquires a stronger mismatch with the copropagating parent interference pattern $\vec{e}_L^*\left(\vec{r}\right) \cdot \vec{e}_s\left(\vec{r}\right)$, thus reducing the efficiency of Brillouin process.

This feature recalls the sound diffraction effect widely discussed in the past in the context of SBS in single-mode optical fibers [45-48]. Indeed, in a single-mode fiber, the sound wave is generated in the fiber core, where the light is localized. So, the sound wave is generated within a small transverse fiber area with the size of $a \sim \lambda_L$ (comparable with the sound wave wavelength $\sim \lambda_L/2n$), and suffers diffraction divergence as it propagates in the fiber. As a result, it runs away from the fiber core, impairing the efficiency of its interaction with the optical fields. This process is important, and affects the SBS process when the time associated with the sound divergence $\tau_D \approx a^2/v\lambda_L$ becomes smaller than the sound relaxation time T_2: $\tau_D < T_2$. In other words, the diffraction time constant τ_D becomes significant and replaces T_2 in the 1-D SBS dynamical equations and expressions for the Brillouin gain spectrum, causing its broadening and thereby suppressing the Brillouin interaction in a single-mode fiber.

In this paper, we have demonstrated that a similar effect could be obtained with the SBS in multimode fibers. When the SBS involves interaction of high-order optical modes, the sound diffraction effect occurs due to the different manner of propagation in the optical fiber of optical and sound waves. The optical fiber supports the waveguide manner of propagation for optical waves only, whereas it remains a volume medium for sound waves (until we ignore its guiding and anti-guiding properties at sound frequencies) [42]. The optical eigenmodes in an optical fiber are expressed through special functions, while the sound eigenmodes remain to be plane waves. As a result, a sound wave generated in some fiber points by the interference pattern produced by a pair of pump and Stokes eigenmodes $\vec{e}_L\left(\vec{r}_\perp\right)$, $\vec{e}_s\left(\vec{r}_\perp\right)$ has a transverse structure $\sim\left\{\vec{e}_L^*\left(\vec{r}_\perp\right)\vec{e}_s\left(\vec{r}_\perp\right)\right\}$ that is not maintained during its further free propagation through the fiber. The mismatch between the sound wave and traveling interference pattern occurs with the typical time $\tau_D = \dfrac{n}{c}\dfrac{4\pi a^2}{\lambda_L\left(u_L^2 + u_S^2\right)}$.

When this mismatch occurs faster than the sound wave decays $\tau_D \succ T_2$, the sound diffraction effect takes charge for the SBS gain spectrum broadening, resulting in suppression of the SBS interaction near the low-frequency spectral peak. In contrast, the sound diffraction effect is not observed with the planar (and rectangle) waveguides, since both optical and sound eigenmodes are plane waves. In this case, a sound wave generated by the interference between pump and Stokes eigenmodes always keeps its resonance with the parent interference pattern, as they both propagate through the fiber.

CONCLUSION

In conclusion, we have studied the SBS interaction in optical fiber implemented with a pair of counter-propagating optical modes. In contrast to the previously reported theoretical considerations [35-37], we use a weakly guided optical fiber model and have managed to build analytical expressions for the SBS gain spectrum (Eq. 9) and sound wave core profile (Eq. 6) eligible for the SBS interaction between two arbitrary modes. Importantly, we have described the sound diffraction effect for SBS in multimode optical fibers, which is similar to that known earlier for SBS in single-mode fibers. It is worth noting that the developed approach could be extended to describe the SBS interaction between groups of modes selectively excited in multimode optical fibers, thus enabling a simplified analysis of the mode conversion processes (including the OPC effect) performed immediately in multimode optical fibers. Additionally, a similar mathematical treatment could be applied to other SBS models employing the descriptions of optical fiber modes expressed through Bessel functions.

Looking to future experiments that have to be performed to verify the theoretical predictions reported in this work, the amplified narrow-band fiber lasers [49-55] combined with the all-digital hologram and phase plate devices [56, 57] could be considered as valuable candidates to serve as critical elements of the experimental setup, enabling the selective excitation of pure single optical modes in multimode fibers, and their de-multiplexing at the fiber output. Direct control of the optical field amplitudes and phases through a flexible SLM used as a holographic filter enables a fast switch of the

excited fiber mode composition. Combining this procedure with a mode-analyzing technique allows the evaluation of the excited mode purity. A feedback control system between the mode analysis and the mode excitation would be essential to minimize the mode excitation errors and compensate for distortions caused by the fiber environment.

We believe our findings will stimulate progress in the significant drive to develop modern imaging and mode-division multiplexing sensor techniques, as discussed in the introduction. In particular, using the properties of the SBS gain spectrum similar to that shown in Fig. 3, the SBS could supply these techniques by selective mode amplification and suppression, resulting in direct optical mode processing performed immediately in multi-mode optical fibers. In addition, this could enable new sensing applications of the optical Vernier effect through employing slightly detuned Brillouin frequency shifts that are naturally implemented to optical modes of different orders, since this is an inherent property of the SBS in optical fiber (Eq. 9). In addition, the forward Brillouin scattering in optical fibers[58-63] could be of particular interest for further studies due to its practical importance for soliton fiber lasers as an effect enabling the stabilization of harmonically mode-locked laser operation and super-mode noise reduction [64-69].

ACKNOWLEDGEMENTS

REFERENCES

[1] Bai, Z., Yuan, H., Liu, Z., Xu, P., Gao, Q., Williams, R. J., Kitzler, O., Mildren, R. P., Wang, Y., and Lu, Z., "Stimulated brillouin scattering materials, experimental design and applications: A review," Optical Materials 75, 626-645 (2018).

[2] Kuzin, E. A., Petrov, M. P., and Fotiadi, A. A., "Phase conjugation by smbs in optical fibers," in Optical phase conjugation, D. P. M. Gower, ed. (Springer-Verlag, 1994), pp. 74-96.

[3] Ostermeyer, M., Kong, H. J., Kovalev, V. I., Harrison, R. G., Fotiadi, A. A., Mégret, P., Kalal, M., Slezak, O., Yoon, J. W., Shin, J. S., Beak, D. H., Lee, S. K., Lü, Z., Wang, S., Lin, D., Knight, J. C., Kotova, N. E., Sträßer, A., Scheikh-Obeid, A., Riesbeck, T., Meister, S., Eichler, H. J., Wang, Y., He, W., Yoshida, H., Fujita, H., Nakatsuka, M., Hatae, T., Park, H., Lim, C., Omatsu, T., Nawata, K., Shiba, N., Antipov, O. L., Kuznetsov, M. S., and Zakharov, N. G., "Trends in stimulated brillouin scattering and optical phase conjugation," Laser and Particle Beams 26 (2008).

[4] Gomes, A. D., Bartelt, H., and Frazão, O., "Optical vernier effect: Recent advances and developments," Laser & Photonics Reviews 15, 2000588 (2021).

[5] Tanaka, Y., and Ozaki, Y., "Brillouin frequency shift measurement with virtually controlled sensitivity," Applied Physics Express 10, 062504 (2017).

[6] Meng, Z., and Yakovlev, V. V., "Optimizing signal collection efficiency of the vipa-based brillouin spectrometer," Journal of Innovative Optical Health Sciences 08, 1550021 (2015).

[7] La Cavera, S., Pérez-Cota, F., Fuentes-Domínguez, R., Smith, R. J., and Clark, M., "Time resolved brillouin fiber-spectrometer," Opt. Express 27, 25064-25071 (2019).

[8] Karampatzakis, A., Song, C. Z., Allsopp, L. P., Filloux, A., Rice, S. A., Cohen, Y., Wohland, T., and Török, P., "Probing the internal micromechanical properties of pseudomonas aeruginosa biofilms by brillouin imaging," npj Biofilms and Microbiomes 3, 20 (2017).

[9] Wang, S., Zhang, W., Yang, N., Ma, R., Zhang, Y., Wang, Z., Zhang, J., and Rao, Y., "High-power multimode random fiber laser for speckle-free imaging," Annalen der Physik 533, 2100390 (2021).

[10] Čižmár, T., and Dholakia, K., "Exploiting multimode waveguides for pure fibre-based imaging," Nature Communications 3, 1027 (2012).

[11] Popov, S. M., Butov, O. V., Bazakutsa, A. P., Vyatkin, M. Y., Chamorovskii, Y. K., and Fotiadi, A. A., "Random lasing in a short er-doped artificial rayleigh fiber," Results in Physics 16, 102868 (2020).

[12] Popov, S. M., Butov, O. V., Chamorovskiy, Y. K., Isaev, V. A., Kolosovskiy, A. O., Voloshin, V. V., Vorob'ev, I. L., Vyatkin, M. Y., Mégret, P., Odnoblyudov, M., Korobko, D. A., Zolotovskii, I. O., and Fotiadi, A. A., "Brillouin lasing in single-mode tapered optical fiber with inscribed fiber bragg grating array," Results in Physics 9, 625-627 (2018).

[13] Popov, S., Butov, O., Kolosovskii, A., Voloshin, V., Vorob'ev, I. L., Isaev, V. A., Vyatkin, M. Y., Fotiadi, A., and Chamorovsky, Y. K., "Optical fibres and fibre tapers with an array of bragg gratings," Quantum Electronics 49, 1127-1131 (2019).

[14] Fotiadi, A. A., and Kiyan, R. V., "Cooperative stimulated brillouin and rayleigh backscattering process in optical fiber," Optics Letters 23, 1805 (1998).

[15] Liew, S. F., Redding, B., Choma, M. A., Tagare, H. D., and Cao, H., "Broadband multimode fiber spectrometer," Optics Letters 41, 2029-2032 (2016).

[16] Redding, B., Popoff, S. M., and Cao, H., "All-fiber spectrometer based on speckle pattern reconstruction," Opt. Express 21, 6584-6600 (2013).

[17] Finlay, M. C., Mosse, C. A., Colchester, R. J., Noimark, S., Zhang, E. Z., Ourselin, S., Beard, P. C., Schilling, R. J., Parkin, I. P., Papakonstantinou, I., and Desjardins, A. E., "Through-needle all-optical ultrasound imaging in vivo: A preclinical swine study," Light: Science & Applications 6, e17103-e17103 (2017).

[18] La Cavera, S., Pérez-Cota, F., Smith, R. J., and Clark, M., "Phonon imaging in 3d with a fibre probe," Light: Science & Applications 10, 91 (2021).

[19] Faustov, A. V., Gusarov, A. V., Mégret, P., Wuilpart, M., Zhukov, A. V., Novikov, S. G., Svetukhin, V. V., and Fotiadi, A. A., "The use of optical frequency-domain reflectometry in remote distributed measurements of the γ-radiation dose," Technical Physics Letters 41, 414-417 (2015).

[20] Fotiadi, A. A., Brambilla, G., Ernst, T., Slattery, S. A., and Nikogosyan, D. N., "Tpa-induced long-period gratings in a photonic crystal fiber: Inscription and temperature sensing properties," Journal of the Optical Society of America B: Optical Physics 24, 1475-1481 (2007).

[21] Brambilla, G., Fotiadi, A. A., Slattery, S. A., and Nikogosyan, D. N., "Two-photon photochemical long-period grating fabrication in pure-fused-silica photonic crystal fiber," Optics Letters 31, 2675 (2006).

[22] Gorshkov, B. G., Yüksel, K., Fotiadi, A. A., Wuilpart, M., Korobko, D. A., Zhirnov, A. A., Stepanov, K. V., Turov, A. T., Konstantinov, Y. A., and Lobach, I. A., "Scientific applications of distributed acoustic sensing: State-of-the-art review and perspective," Sensors 22, 1033 (2022).

[23] Caucheteur, C., Fotiadi, A., Megret, P., Slattery, S. A., and Nikogosyan, D. N., "Polarization properties of long-period gratings prepared by high-intensity femtosecond 352-nm pulses," IEEE Photonics Technology Letters 17, 2346-2348 (2005).

[24] Murshid, S., Grossman, B., and Narakorn, P., "Spatial domain multiplexing: A new dimension in fiber optic multiplexing," Optics & Laser Technology 40, 1030-1036 (2008).

[25] Caucheteur, C., Villatoro, J., Liu, F., Loyez, M., Guo, T., and Albert, J., "Mode-division and spatial-division optical fiber sensors," Adv. Opt. Photon. 14, 1-86 (2022).

[26] Weng, Y., Ip, E., Pan, Z., and Wang, T., "Advanced spatial-division multiplexed measurement systems propositions-from telecommunication to sensing applications: A review," Sensors (Basel) 16 (2016).

[27] Weng, Y., Wang, T., and Pan, Z., "Multi-functional fiber optic sensors based on mode division multiplexing," Optical Materials Express 7, 1917-1933 (2017).

[28] Zhang, Z., Lu, Y., Pan, Y., Bao, X., and Chen, L., "Trench-assisted multimode fiber used in brillouin optical time domain sensors," Opt. Express 27, 11396-11405 (2019).

[29] Shwartz, S., Golub, M. A., and Ruschin, S., "Excitation of mode groups in multimode fibers with the aid of diffractive optics," IEEE Photonics Technology Letters 28, 1763-1766 (2016).

[30] Schulze, C., Wilde, J., Brüning, R., Schröter, S., and Duparré, M., "Measurement of effective refractive index differences in multimode optical fibers based on modal decomposition," Optics Letters 39, 5810-5813 (2014).

[31] Rodgers, B. C., Russell, T. H., and Roh, W. B., "Laser beam combining and cleanup by stimulated brillouin scattering in a multimode optical fiber," Optics Letters 24, 1124-1126 (1999).

[32] Kuzin, E., Petrov, M., and Fotiadi, A., "Fiber-optic stimulated-brillouin-scattering amplifier," Soviet Physics Technical Physics 33, 206-209 (1988).

[33] Minardo, A., Bernini, R., and Zeni, L., "Experimental and numerical study on stimulated brillouin scattering in a graded-index multimode fiber," Opt. Express 22, 17480-17489 (2014).

[34] Snyder, A. W., and Love, J., [Optical waveguide theory], Springer Science & Business Media (2012).

[35] Kobyakov, A., Sauer, M., and Chowdhury, D., "Stimulated brillouin scattering in optical fibers," Adv. Opt. Photon. 2, 1-59 (2010).

[36] Greenberg, A. P., Ma, Z., and Ramachandran, S., "Angular momentum driven dynamics of stimulated brillouin scattering in multimode fibers," Opt. Express 30, 29708-29721 (2022).

[37] Wisal, K., Warren-Smith, S. C., Chen, C.-W., Behunin, R., Cao, H., and Stone, A. D., "Generalized theory of sbs in multimode fiber amplifiers," in Physics and Simulation of Optoelectronic Devices XXX(SPIE2022), p. PC1199504.

[38] Iezzi, V. L., Loranger, S., Harhira, A., Kashyap, R., Saad, M., Gomes, A., and Rehman, S., "Stimulated brillouin scattering in multi-mode fiber for sensing applications," in 2011 7th International Workshop on Fibre and Optical Passive Components(IEEE2011), pp. 1-4.

[39] Beugnot, J.-C., and Laude, V., "Electrostriction and guidance of acoustic phonons in optical fibers," Physical Review B 86 (2012).

[40] Godet, A., Ndao, A., Sylvestre, T., Pecheur, V., Lebrun, S., Pauliat, G., Beugnot, J.-C., and Phan Huy, K., "Brillouin spectroscopy of optical microfibers and nanofibers," Optica 4, 1232 (2017).

[41] Stiller, B., Delqué, M., Beugnot, J. C., Lee, M. W., Mélin, G., Maillotte, H., Laude, V., and Sylvestre, T., "Frequency-selective excitation of guided acoustic modes in a photonic crystal fiber," Opt. Express 19, 7689-7694 (2011).

[42] Fotiadi, A., Rafailov, E., Korobko, D., Megret, P., Bykov, A., and Meglinski, I., "Brillouin interaction between two optical modes selectively excited in weakly guiding multimode optical fibers," Sensors (Basel) 23 (2023).

[43] Gaeta, A. L., and Boyd, R. W., "Stochastic dynamics of stimulated brillouin scattering in an optical fiber," Physical Review A 44, 3205 (1991).

[44] Starunov, V. S., and Fabelinskii, I. L., "Stimulated mandel'shtam–brillouin scattering and stimulated entropy (temperature) scattering of light," Uspekhi Fizicheskikh Nauk 98, 441-491 (1969).

[45] Zel'dovich, B. Y., and Pilipetskiĭ, A. N., "Influence of sound diffraction on stimulated brillouin scattering in a single-mode waveguide," Soviet Journal of Quantum Electronics 16, 546 (1986).

[46] Zel'dovich, B. Y., and Pilipetskii, A. N., "Role of a "soundguide" and "antisoundguide" in stimulated brillouin scattering in a single-mode waveguide," Soviet Journal of Quantum Electronics 18, 818 (1988).

[47] Grimalsky, V., Gutierrez-D, E., Koshevaya, S., and Mansurova, S., "Modulation instability of the stimulated brillouin scattering in fibers in a presence of acoustic diffraction," Optik 114, 134-138 (2003).

[48] Grimalsky, V., Koshevaya, S., Burlak, G., and Salazar-H, B., "Dynamic effects of the stimulated brillouin scattering in fibers due to acoustic diffraction," Journal of the Optical Society of America B 19, 689 (2002).

[49] Spirin, V. V., Bueno Escobedo, J. L., Korobko, D. A., Mégret, P., and Fotiadi, A. A., "Dual-frequency laser comprising a single fiber ring cavity for self-injection locking of dfb laser diode and brillouin lasing," Opt. Express 28, 37322-37333 (2020).

[50] Spirin, V. V., Bueno Escobedo, J. L., Korobko, D. A., Mégret, P., and Fotiadi, A. A., "Stabilizing dfb laser injection-locked to an external fiber-optic ring resonator," Opt. Express 28, 478-484 (2020).

[51] Lopez-Mercado, C. A., Korobko, D. A., Zolotovskii, I. O., and Fotiadi, A. A., "Application of dual-frequency self-injection locked dfb laser for brillouin optical time domain analysis," Sensors 21, 6859 (2021).

[52] Korobko, D. A., Zolotovskii, I. O., Panajotov, K., Spirin, V. V., and Fotiadi, A. A., "Self-injection-locking linewidth narrowing in a semiconductor laser coupled to an external fiber-optic ring resonator," Optics Communications 405, 253-258 (2017).

[53] Korobko, D., Zolotovskii, I., Svetukhin, V., Zhukov, A., Fomin, A., Borisova, C., and Fotiadi, A., "Detuning effects in brillouin ring microresonator laser," Opt. Express 28, 4962-4972 (2020).

[54] Preda, C. E., Fotiadi, A. A., and Megret, P., "Numerical approximation for brillouin fiber ring resonator," Opt Express 20, 5783-5788 (2012).

[55] Spirin, V. V., Bueno Escobedo, J. L., Miridonov, S. V., Maya Sánchez, M. C., López-Mercado, C. A., Korobko, D. A., Zolotovskii, I. O., and Fotiadi, A. A., "Sub-kilohertz brillouin fiber laser with stabilized self-injection locked dfb pump laser," Optics & Laser Technology 141, 107156 (2021).

[56] Flamm, D., Schulze, C., Naidoo, D., Schroter, S., Forbes, A., and Duparre, M., "All-digital holographic tool for mode excitation and analysis in optical fibers," Journal of Lightwave Technology 31, 1023-1032 (2013).

[57] Liñares, J., Montero-Orille, C., Moreno, V., Mouriz, D., Nistal, M. C., and Prieto-Blanco, X., "Ion-exchanged binary phase plates for mode multiplexing in graded-index optical fibers," Applied Optics 56, 7099-7106 (2017).

[58] Shelby, R. M., Levenson, M. D., and Bayer, P. W., "Guided acoustic-wave brillouin scattering," Physical Review B 31, 5244-5252 (1985).

[59] Shelby, R., Levenson, M., and Bayer, P., "Resolved forward brillouin scattering in optical fibers," Physical review letters 54, 939 (1985).

[60] Liu, Y., Ning, Y., Gu, Y., Chen, P., Jiang, K., Wang, L., You, Y., He, W., and Chou, X., "Ultra-narrow linewidth dual-cavity opto-mechanical microwave oscillator based on radial guided acoustic modes of single-mode fiber," Applied Physics Letters 122, 041107 (2023).

[61] Sánchez, L. A., Díez, A., Cruz, J. L., and Andrés, M. V., "High accuracy measurement of poisson's ratio of optical fibers and its temperature dependence using forward-stimulated brillouin scattering," Opt. Express 30, 42-52 (2022).

[62] Sánchez, L. A., Díez, A., Cruz, J. L., and Andrés, M. V., "Recent advances in forward brillouin scattering: Sensor applications," in Sensors(2023).

[63] Sánchez, L. A., Díez, A., Cruz, J. L., and Andrés, M. V., "Efficient interrogation method of forward brillouin scattering in optical fibers using a narrow bandwidth long-period grating," Optics Letters 45, 5331-5334 (2020).

[64] Ribenek, V. A., Stoliarov, D. A., Korobko, D. A., and Fotiadi, A. A., "Pulse repetition rate tuning of a harmonically mode-locked ring fiber laser using resonant optical injection," Optics Letters 46, 5687-5690 (2021).

[65] Ribenek, V. A., Stoliarov, D. A., Korobko, D. A., and Fotiadi, A. A., "Mitigation of the supermode noise in a harmonically mode-locked ring fiber laser using optical injection," Optics Letters 46, 5747-5750 (2021).

[66] Ribenek, V. A., Korobko, D. A., Fotiadi, A. A., and Taylor, J. R., "Supermode noise mitigation and repetition rate control in a harmonic mode-locked fiber laser implemented through the pulse train interaction with co-lased cw radiation," Optics Letters 47, 5236-5239 (2022).

[67] Korobko, D. A., Ribenek, V. A., Itrin, P. A., and Fotiadi, A. A., "Birth and annihilation of solitons in harmonically mode-locked fiber laser cavity through continuous wave injection," Optical Fiber Technology 75, 103216 (2023).

[68] Korobko, D. A., Ribenek, V. A., Itrin, P. A., Stoliarov, D. A., and Fotiadi, A. A., "Polarization maintaining harmonically mode-locked fiber laser with suppressed supermode noise due to continuous wave injection," Optics & Laser Technology 162, 109284 (2023).

[69] Kbashi, H. J., Sergeyev, S. V., Al-Araimi, M., Rozhin, A., Korobko, D., and Fotiadi, A., "High-frequency vector harmonic mode locking driven by acoustic resonances," Optics Letters 44, 5112-5115 (2019).